Journal of Non-Newtonian Fluid Mechanics 173–174 (2012) 21–29

Contents lists available at SciVerse ScienceDirect

Journal of Non-Newtonian Fluid Mechanics

journal homepage: http://www.elsevier.com/locate/jnnfm

# Experimental investigation of non-Newtonian liquid flow in microchannels

G.H. Tang *, Y.B. Lu, S.X. Zhang, F.F. Wang, W.Q. Tao

*MOE Key Laboratory of Thermo-Fluid Science and Engineering, School of Energy and Power Engineering, Xi'an Jiaotong University, Xi'an 710049, PR China*

ARTICLE INFO

*Article history:*
Received 4 October 2011
Received in revised form 3 February 2012
Accepted 6 February 2012
Available online 15 February 2012

*Keywords:*
Non-Newtonian liquid
Microchannels
PAM solution
Hydrophobic
Experimental study

ABSTRACT

Investigation on non-Newtonian fluid flow in microchannels is of both fundamental interest and practical significance. Flow characteristics of deionized water and the PAM solution over a wide range of Reynolds numbers in fused silica microtubes with diameters from 75 to 250 μm, fused silica square microchannels with equivalent diameters of 75 and 100 μm, and stainless steel microtubes with diameters from 120 to 300 μm, were studied experimentally. The obtained mass flow rate and friction factor for deionized water in smooth fused silica microchannels were in good agreement with theoretical predictions for conventional-sized channels while the deviation for stainless steel microtubes was observed due to the roughness. Friction factors of the PAM solution were much higher than conventional theoretical predictions. Flow behaviors of deionized water and the PAM solution under hydrophobic condition are also studied experimentally. The mass flow rate increased in hydrophobic microchannels compared to untreated microchannels. The drag reduction in hydrophobic channels is greater for rough stainless steel microtubes than for smooth fused silica channels. The effect of surface wettability on the shear thinning PAM solution is also observed to be more evident than on the Newtonian deionized water.



## 1. Introduction

In recent years, research on microscale liquid flow has obtained great attentions due to the rapid development of micro-electro-mechanical-systems (MEMSs) and micro processing technology. Microsystems has been widely used in industry and biological medicine, such as the DNA microarray and sorting, sample pretreatment and analysis, cell separation and detection, environmental testing, capillary viscometer and so on [1–5]. Many scholars have made a lot of experiments on the fundamental single phase liquid microchannel flow [6–19]. However, most of them are limited to simple Newtonian fluids such as water, and refrigerant fluids. Few experimental researches on non-Newtonian fluid flow in microchannels have been conducted [5,20]. Koo and Kleinstreuer [21] analyzed that the non-Newtonian fluid effect on the microflow friction factor is quite significant. Most recently, surface wettability on liquid flow in microchannels has also been experimentally investigated since hydrophobic surfaces (non-wetting condition) have been demonstrated to be capable of reducing drag in micro and nanofluidic applications [22–31]. However, to the authors' best knowledge, all these studies were also focused on Newtonian fluids. Non-Newtonian fluid flow has broad applications in both our daily life and various industries. In particular, the flow behavior of non-Newtonian fluid in microchannels is of high interest in practical applications such as sample collection, dispensing, reaction, detection, mixing, and separation of various biological and chemical species in microchips integrated with fluidic pumps, valves, and sensors, as well as in capillary viscometer to measure the non-Newtonian viscosity of chemical and biological polymeric solutions. The purpose of this work is to experimentally examine the non-Newtonian fluid flow characteristics in various microchannels with and without wettability treatment.

## 2. Experimental method

The experimental test system is depicted schematically in Fig. 1. The detailed descriptions for components and measurement apparatus are listed in Table 1. A compressed nitrogen gas of high purity connected to the reservoir tank is employed to pressurize the working fluid through the filter, test microchannel, flow meter, and electronic balance in sequence. A 0.5 μm filter is used to prevent the microchannel from possible clotting. The pressure is measured by using pressure transducers with different ranges. The electronic balance is used to measure the mass flow rate. Also, the volume flow rate is measured by using volume flow meters with different ranges. Two thermocouples at test channel inlet and outlet are distributed to measure the liquid temperature for physical properties. The flow meters, pressure transducers, thermocouples, and electronic balance are all connected to a computerized data acquisition system.

Three types of microchannels, fused silica tubes (FSTs), fused silica square channels (FSCs), stainless steel tubes (SSTs), listed in Table 2, are tested in the experiment. The lengths of the tested

* Corresponding author. Tel.: +86 29 82665319; fax: +86 29 82669106.
*E-mail address:* ghtang@mail.xjtu.edu.cn (G.H. Tang).

0377-0257/$ - see front matter © 2012 Elsevier B.V. All rights reserved.
doi:10.1016/j.jnnfm.2012.02.001

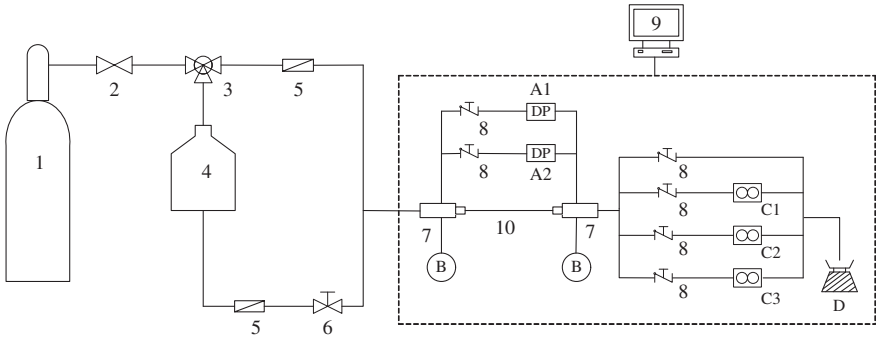


**Fig. 1.** Schematic of the experimental loop.

ten microchannels are all fixed at $L$ = 100 mm. The typical photos of cross-section and longitudinal-section by a scanning electron microscope (SEM) are shown in Fig. 2 and we can observe that the inner surface of stainless steel pipe is quite rough and irregularly structured. By using light-section microscope, the absolute average surface roughness of the four test stainless steel microtubes is 7 μm. But the inner surface of the fused silica tubes and fused silica square channels is very smooth with relative roughness far less than 1%. The surface relative roughness of the tested stainless steel tubes is significantly larger than that for fused silica channels due to different machining method.

Deionized water (DI water) and the polyacrylamide (PAM) solution are used as the working fluid in the experiment. The deionized water as a type of typical Newtonian fluid, is employed to check the reliability of experimental system. The PAM in this study is a water-soluble polymer with molecular weight (MW) of five million, and a type of typical shear thinning power law fluid.

For non-Newtonian fluid, rheological parameters are needed to evaluate the rheological characteristics. We used the rotational cylinder viscometer of American Brookfield R/S plus series to measure the viscosity of the PAM solution (The accuracy for viscosity is 1%). The constitutive equations of non-Newtonian power law fluid can be written as

$$\tau = k\dot{\gamma}^n \tag{1}$$

with shear thinning fluid $n < 1$, and shearing thickening fluid $n > 1$.The power law equation reduces to the constitutive equation of Newtonian fluid with $n = 1$and $k = \mu$. Here $\tau$ is the shear force; $\dot{\gamma}$ is the shear rate. $\mu$ is the dynamic viscosity of the Newtonian fluid. The rheological properties of power law fluid are relevant to the power law index $n$ and consistency coefficient $k$.

For power law fluids, Kozicki et al. [32] introduced a new generalized Reynolds number $\mathrm{Re}^*$ which is so defined that the relationship $f = 64/\mathrm{Re}^*$ is applicable to fully developed laminar flow in arbitrary channel of constant cross-section. For power law fluid flow, the generalized Reynolds number and mass flow rate from conventional theory are expressed as Eqs. (2) and (3), respectively.

$$\mathrm{Re}^* = \frac{\rho D_h^n u^{2-n}}{k}\left(\frac{n}{a+bn}\right)^n \cdot 8^{1-n} \tag{2}$$

$$Q_m = \rho A\left(\frac{\Delta p}{kL}\right)^{\frac{1}{n}} \frac{n}{a+bn} D_h^{\frac{1+3n}{n}} \left(\frac{1}{2}\right)^{\frac{3n+2}{n}} \tag{3}$$

where $\Delta p$ is the pressure difference between the test channel inlet and outlet; $\rho$ is the fluid density; $D_h$ is the equivalent diameter of channel; $u$ is the average velocity. Similarly, for square cross-sectional channel flow; $A$ is the cross-sectional area of test channel. The constants $a = 0.25$ and $b = 0.75$ for circular pipes and $a = 0.2121$ and $b = 0.6766$ for square cross-sectional channel [32]. If $n = 1$ and $k = \mu$, Eq. (2) recovers to the Reynolds number Re for Newtonian fluid flow and Eq. (3) also recovers to the Newtonian fluid flow mass flow rate. Note that Eq. (3) is limited to fully developed laminar flow. The experimental friction factor is calculated as

$$f_{\mathrm{exp}} = \frac{2D_h\Delta p}{\rho u^2 L} = \frac{2D_h\rho A^2\Delta p}{Q_{m,\mathrm{exp}}^2 L} \tag{4}$$

**Table 1**
Experimental flow loop components.

| Label | Description | Manufacturer/model | Range | Precision |
|---|---|---|---|---|
| 1 | Gas tank | MESSER | 15 MPa | |
| 2 | Pressure regulator | Shanghai regulator factory/YQD-6 | | |
| 3 | Three-way valve | SS-43XS4 | | |
| 4 | Liquid storage tank | | | |
| 5 | Filter | Swagelok /SS-4F-05 | | 0.5 μm |
| 6 | Precision regulator | Swagelok /SS-SS4 | | |
| 7 | Connection adapter for test section | | | |
| 8 | Plug valve | Swagelok /SS-4P4T | | |
| 9 | Data acquisition system | | | |
| 10 | Test section | FST/SST/FSC | | |
| A1 | Pressure transducer | 1151DP622 | 0–300 kPa | 0.25% |
| A2 | Pressure transducer | 1151DP722 | 0–2068 kPa | 0.25% |
| B | Thermocouples | T-type copper-constantan/omega | 0–200 °C | 0.5 K |
| C1 | Volumetric flow meter | Cole-parmer/3291601 | 0–1 ml/min | 2% |
| C2 | Volumetric flow meter | Cole-parmer/3291602 | 0–5 ml/min | 2% |
| C3 | Volumetric flow meter | Cole-parmer/3291606 | 0–50 ml/min | 2% |
| D | High precision electronic balance | Mettler Toledo/ AL204 | 0–210 g | 0.1 mg |

**Table 2**
Dimensions of the test microchannels.

| Test channel | Equivalent diameter $D_h \pm 1$ μm |
|---|---|
| FST250 | 250.00 |
| FST200 | 201.44 |
| FST100 | 102.74 |
| FST75 | 74.36 |
| FSC100 | 100.25 |
| FSC75 | 75.34 |
| SST300 | 300.00 |
| SST260 | 260.00 |
| SST170 | 172.00 |
| SST120 | 119.09 |

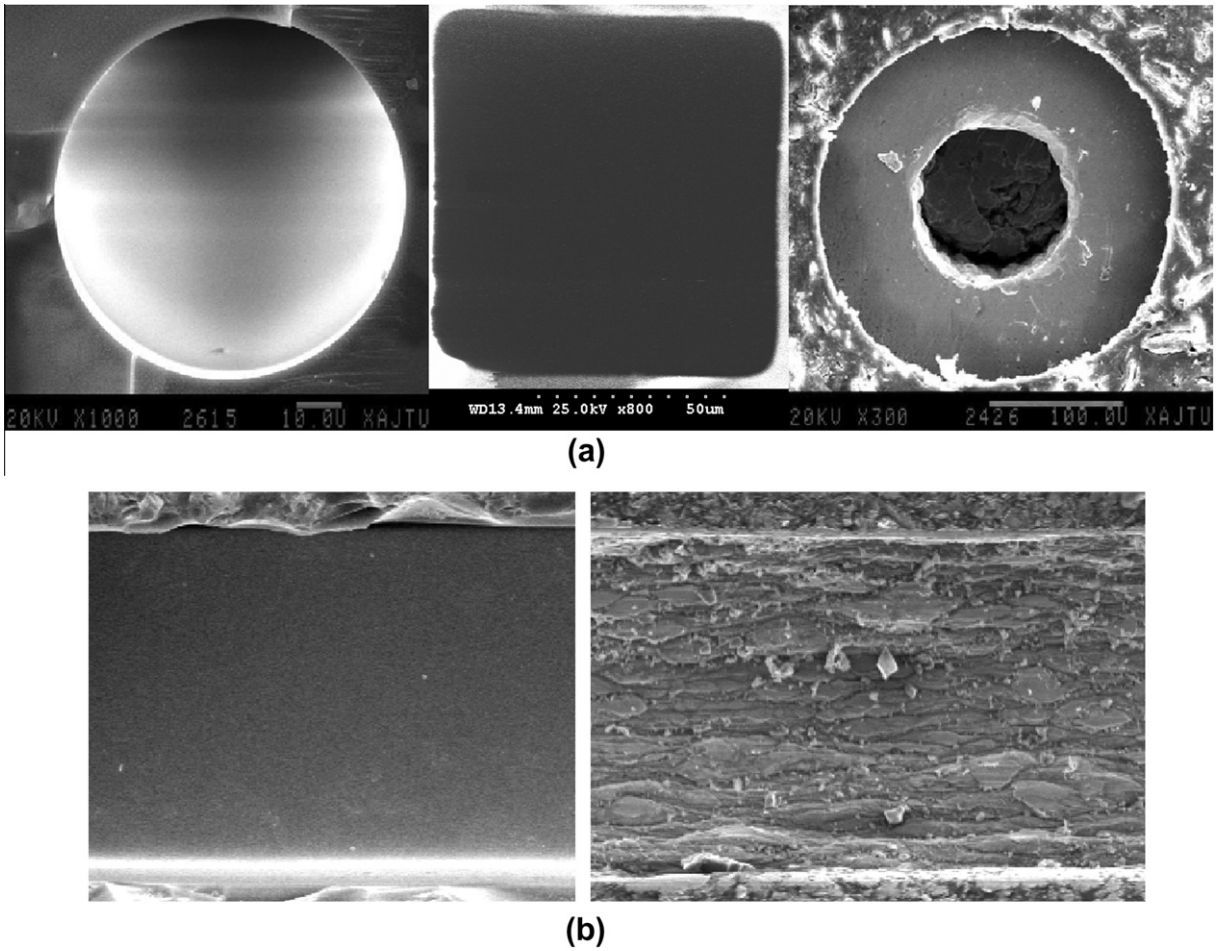


**Fig. 2.** SEM images of three typical tested microchannels. (a) Cross-sections of FST75, FSC100, and SST120 from left to right; (b) longitudinal profiles for the fused silica surface (left) and stainless steel surface (right).

where $L$ is the length of the test channel; $Q_{m,\exp}$ is the measured mass flow rate in the experiment.

The uncertainty analysis was performed to assess the accuracy of measurement. Calculated values such as Reynolds number and friction factor have an uncertainty based on individual uncertainties of each measured value used in the calculation. The uncertainty of the Reynolds number and the friction factor, generally denoted by $\delta y$, is determined by the root-sum-square expression,

$$y = f(x_1, x_2, \ldots, x_N) \tag{5}$$

$$\delta y = \sqrt{\left(\frac{\partial f}{\partial x_1}\delta x_1\right)^2 + \left(\frac{\partial f}{\partial x_2}\delta x_2\right)^2 + \ldots \left(\frac{\partial f}{\partial x_N}\delta x_N\right)^2} \tag{6}$$

where $\delta x_1$ to $\delta x_N$ are the measurement uncertainties for each device. The uncertainties of measurement devices for flow parameters are listed in Table 1 and those for the channel dimension are listed in Table 2. By applying Eq. (6), the calculated maximum relative uncertainties for Newtonian flow Reynolds number, non-Newtonian flow Reynolds number, and friction factor in the experiment are listed in Table 3.

## 3. Results and discussion

First, the deionized water and the PAM solution (1000 wppm) in untreated microchannels are tested in the experiment. The mass flow rate and the pressure drop through the test channels are measured and then the Reynolds number (or generalized Reynolds number) and friction factor can be calculated from the above equations. The values of $k$ and $n$ for the PAM solution vary slightly with the experimental temperature T in each case and we just present here the average by using the rotational cylinder viscometer: $T$ = 15.9 °C, $k$ = 0.00799, and $n$ = 0.8073. Note that after uncertainty analysis the average measurement uncertainty in the present experiment for $k$ and $n$ is 4.37% and 0.75%, respectively.

As can seen from Figs. 3 and 4, for deionized water flow, the experimental results in smooth fused silica tubes and fused silica square channels are in good agreement with conventional

**Table 3**
Uncertainty analysis of the test channels.

| Test channel | $\Delta Re/Re$ (%) | $\Delta Re^*/Re^*$ (%) | $\Delta f/f$ (%) | Reynolds number range |
|---|---|---|---|---|
| FST250 | 0.89 | 6.42 | 2.02 | 2–981 |
| FST200 | 1.11 | 4.15 | 2.53 | 2–843 |
| FST100 | 2.18 | 4.80 | 4.89 | 1–123 |
| FST75 | 3.01 | 5.83 | 6.74 | 1–26 |
| FSC100 | 2.23 | 5.50 | 5.01 | 6–343 |
| FSC75 | 2.97 | 6.01 | 6.66 | 6–171 |
| SST300 | 0.75 | 6.89 | 1.74 | 202–2284 |
| SST260 | 0.86 | 4.75 | 1.99 | 3–2275 |
| SST170 | 1.30 | 4.52 | 2.95 | 6–684 |
| SST120 | 1.88 | 6.59 | 4.23 | 2–124 |

theoretical predictions ($f = 64/Re$ in Fig. 3 and $f = 56.88/Re$ in Fig. 4) obtained by solving the Navier–Stokes equations for fully developed Newtonian flow. The increase in friction factor above theoretical predictions at high flow rates is mainly due to inertial losses and entrance length effects, which were not included in the theory. The deviation from theory gets more obvious for larger dimension channels since the entrance length increases as the channel size and Reynolds number increase. However, as shown in Fig. 5, the obtained friction factors in stainless steel channels depart obviously from conventional theory predictions and the deviation gets larger as the tube diameter decreases, which is mainly attributed to the surface roughness. The measured relative roughness height is 2.3%, 2.7%, 4.1%, and 5.9% for the four stainless steel tubes of $D = 300$, 260, 172, and 119 μm, respectively. The large surface roughness results in the much higher flow friction factor and the observed roughness distribution in the microchannel inner surface is much denser than conventional channels. The deviation from the conventional theory prediction due to roughness even in the laminar region is confirmed with results from [33–35]. The result demonstrates that electrostatic forces do not appear to play an important role in the present experiments for deionized water flow, in spite of the large ratio of surface area to volume, which confirms that the electrostatic effect on Newtonian fluid flow is not significant by numerical analysis [36]. Generally the surface roughness dominates the flow in the cases of increased flow resistance. However, for the PAM solution, we can see that the experimental friction factors in the three types of microchannels are all larger than conventional theory predictions ($f = 64/Re^*$ in Figs. 3 and 4), in spite of the quite smooth inner surface for fused silica channels. The dimension-dependence of the increased friction factor is not obviously observed for the tested fused silica circular microtubes and square microchannels. However, the friction factor for the PAM solution flow in the four stainless steel microchannels in Fig. 5 increases as the channel dimension decreases, indicating the roughness effect again.

The mass flow rate against pressure drop for the 10 test microchannels is depicted in Fig. 6. We can see that for deionized water flow in smooth fused silica circular microtubes and square microchannels, the measured results agree well with conventional theory predictions, though the entrance length effect causes the curve to deviate from the conventional theory prediction at large pressure drops and large dimension channels. The data for stainless steel tubes also reveals the roughness effect. Similar to the friction factor, the obtained mass flow rates for the PAM solution are all lower than conventional theory predictions calculated with Eq. (3) or Eq. (5). At the same pressure drop, the mass flow rate is also lower than that of the DI water flow. This result is in consistence with the experimental data by Wilding et al. [20], who found that the pressure required to achieve a given flow rate increased as the complexity and viscosity of the biological fluid increased and was larger than that for the distilled water. The obviously reduced mass flow rate or increased friction factor for the PAM solution flow is probably caused by the so-called electroviscous effect on liquid flow in microchannels. It is known that the interaction of the electrostatic charged solid wall and the charged ions in the liquid results in the electrical double layers in the liquid flow (EDL). The presence of EDL induces an electrokinetic potential in the pressure-driven flow and a streaming potential which generates a conduction electrical current. And hence part of the liquid is pulled by the ions to flow opposite to the streamwise direction, causing an increased flow resistance. However, the electroviscous effect on Newtonian fluid and shear thickening fluid is not so obvious compared to shear thinning fluid and can be usually neglected, as numerically demonstrated by Tang et al. [36]. The present diverged experimental results between Newtonian DI water flow and shear thinning PAM solution flow in microchannels are consistent with the numerical analysis. Another possible reason could arise from

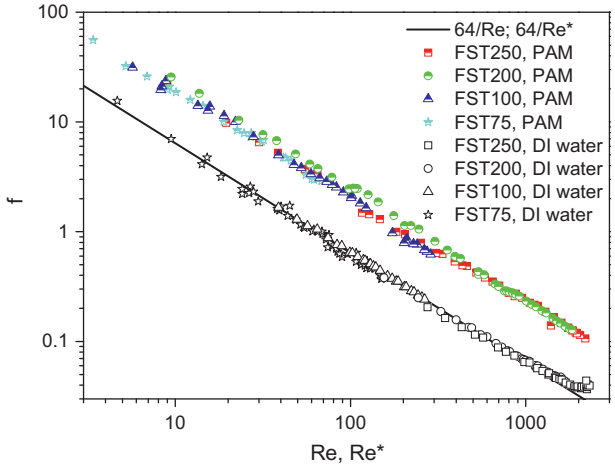


**Fig. 3.** Friction factors for the DI water and PAM solution flow in fused silica circular microtubes.

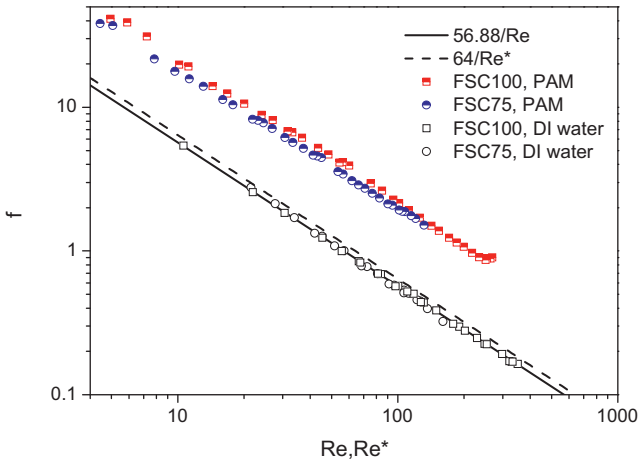


**Fig. 4.** Friction factors for the DI water and PAM solution flow in fused silica square microchannels.

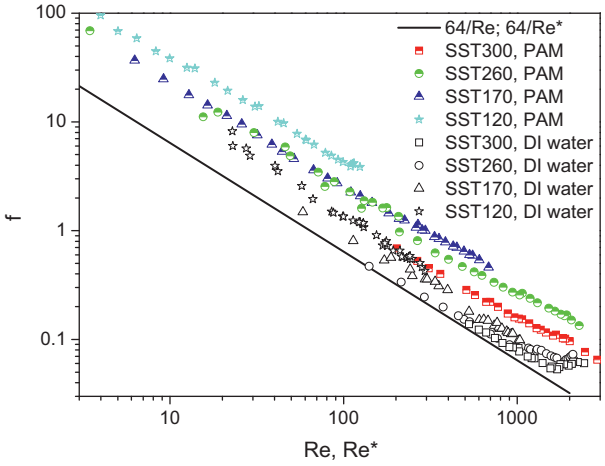


**Fig. 5.** Friction factors for the DI water and PAM solution flow in fused stainless steel circular microtubes.

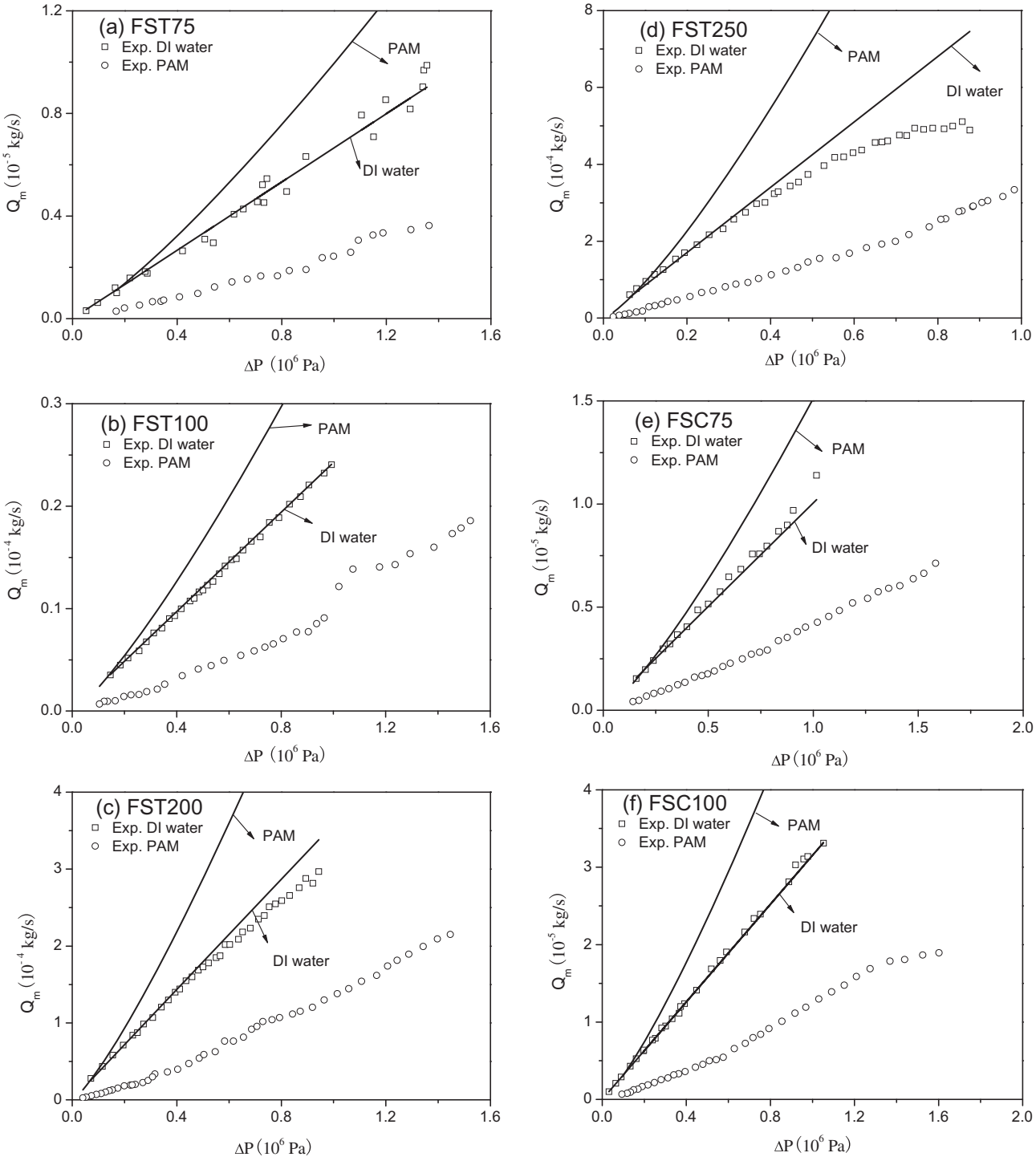


**Fig. 6.** Mass flow rates for the DI water and PAM solution flow in untreated microchannels. Solid lines are conventional theory predictions for fully developed laminar flow. Symbols are experimental data.

measured rheological data. Generally the commercial rotational rheometers can only achieve shear rates as high as $10^3\ s^{-1}$. In our rheology measurement the maximum shear rate is $5000\ s^{-1}$, however, the shear rate for microchannel flow can be as high as $10^6\ s^{-1}$ [4]. In the present experiment, the calculated shear rates are up to $2.8 \times 10^5$, $1.7 \times 10^5$, and $2.4 \times 10^5\ s^{-1}$ for smooth circular pipes, square microchannels, and rough stainless steel pipes, respectively. The power-law fit is probably not appropriate over the range of shear rates experienced in the microchannel. In addition, the inhomogeneous shear field in the microchannel flow also probably caused the deviation of the measurement from the real rheological properties. Surely more theoretical work such as atomistic-continuum hybrid simulation [37] is needed to validate the experimental results.

Solid surface wettability is closely related with adsorption, adhesion, lubrication, friction, and many other physical and chemical processes, which is mainly decided by the surface energy and surface micro or nanostructures. For fluid flow in microchannel

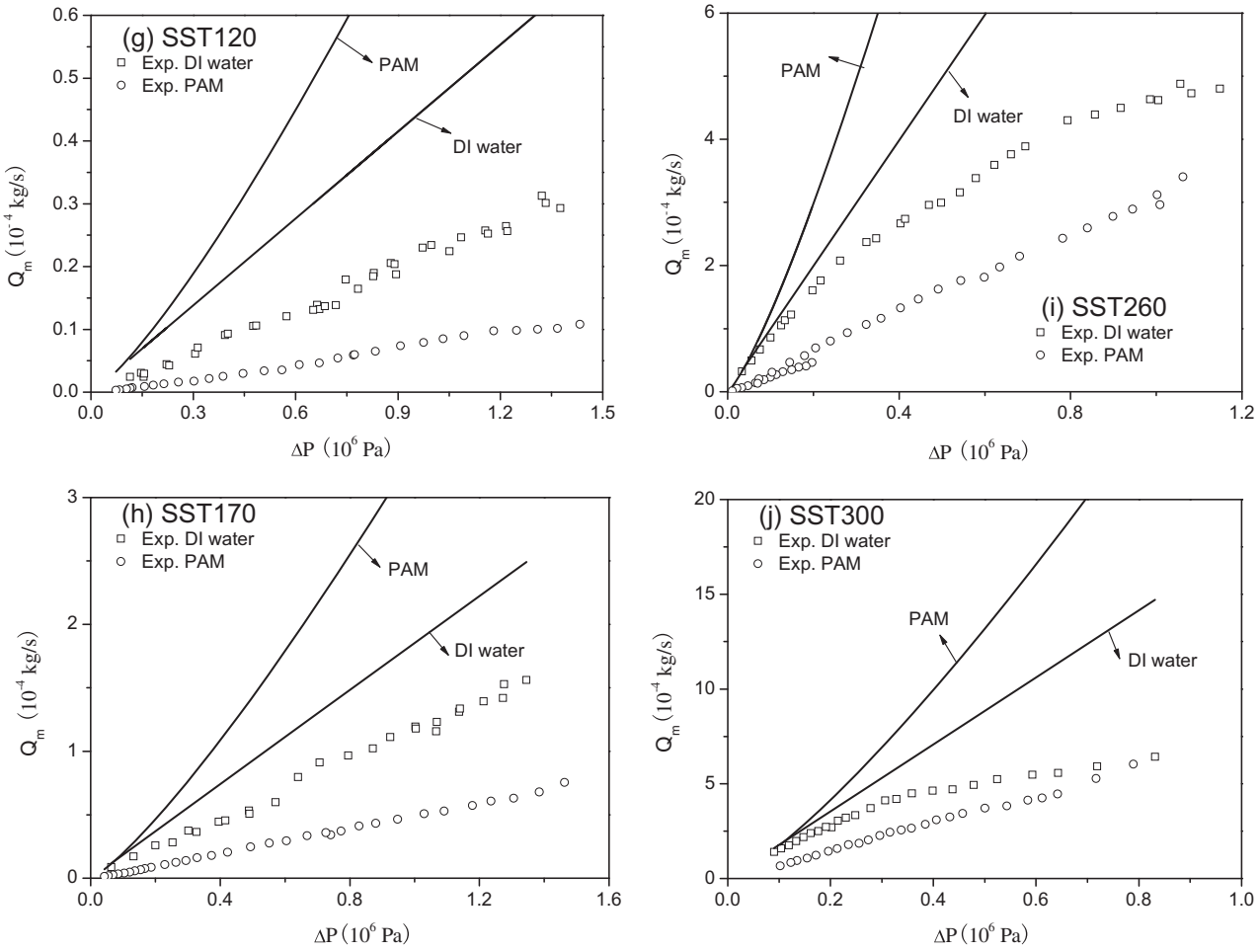


**Fig. 6** (*continued*)

devices, large flow pressure drop as a key factor has restricted the application of microsystem. Therefore, modification of the channel surface can change the channel surface wettability in order to achieve lower flow resistance. However, the non-Newtonian flow in microchannels with wettability processed surface has not ever been reported as yet. The study will be of important significance for the practical application of microfluidic devices.

Reduced free energy of solid surface can enhance the surface hydrophobic nature. The surface modification was completed in a supercritical fluid reactor based on the semi-continuous supercritical phase reaction surface modification process. A hydrophobic solution (Silane solution: 10% Methyl trimethoxysilane + 5% Dimethoxy dimethyl silane) of easy to pyrolysis and low dielectric was grafted onto the solid surface to remove the hydroxyl during a certain temperature (250 °C), pressure (3 MPa), and time (2 h).

Fig. 7 shows the mass flow rate against pressure drop for DI water flow and the PAM solution flow. Similarly, the values of $k$ and $n$ for the PAM solution vary slightly with the experimental temperature $T$ and the average ones are: $T = 23.2$ °C, $k = 0.01086$, and $n = 0.7929$. However, we do not use the rheological data for calculation and just present the tested pressure drop and mass flow rate in this section in order to exclude the possible effect of measured rheological properties. The corresponding flow rate in untreated microchannels is also presented for comparison. We can see that at the same pressure drop, the mass flow rate increases in the hydrophobic microchannels compared to the untreated channel flow. It can also be observed that the gain for stainless steel microtubes is more evident than that in the fused silica channels. If calculating the product of friction factor and Reynolds number, it is found that the maximum drag reduction is up to 43% for DI water flow and 57% for the PAM solution flow, both occurring in the microchannel of SST120. On the whole, the mass flow rate augment gets larger as the channel dimension decreases, since the surface hydrophobic nature changes generally more markedly for smaller dimension during the same surface treatment process.

We know that the surface wettability is mainly decided by both the surface free energy and surface microstructure. For smooth fused silica microchannels, the hydrophobic nature is obtained mainly by changing the surface free energy and the modification is quite limited. However, the microstructure of surface roughness is more efficient to the surface wettability. According to the Cassie model [38], residual air in rough structures causes liquid–air interfaces due to the hydrophobic nature and these interfaces result in large apparent slip at the boundary. The improved contact angle between the droplet of the liquid and the surface can be expected up to larger than 150°, say, super-hydrophobic surface, though the contact angle is not measured because it is coated on the inner surface. Thus the observed mass flow rate increases more in hydrophobic stainless steel microtubes compared to the hydrophobic smooth microchannels. In addition, we can also compare the results between the DI water and PAM solution in Fig. 7. The mass flow rate

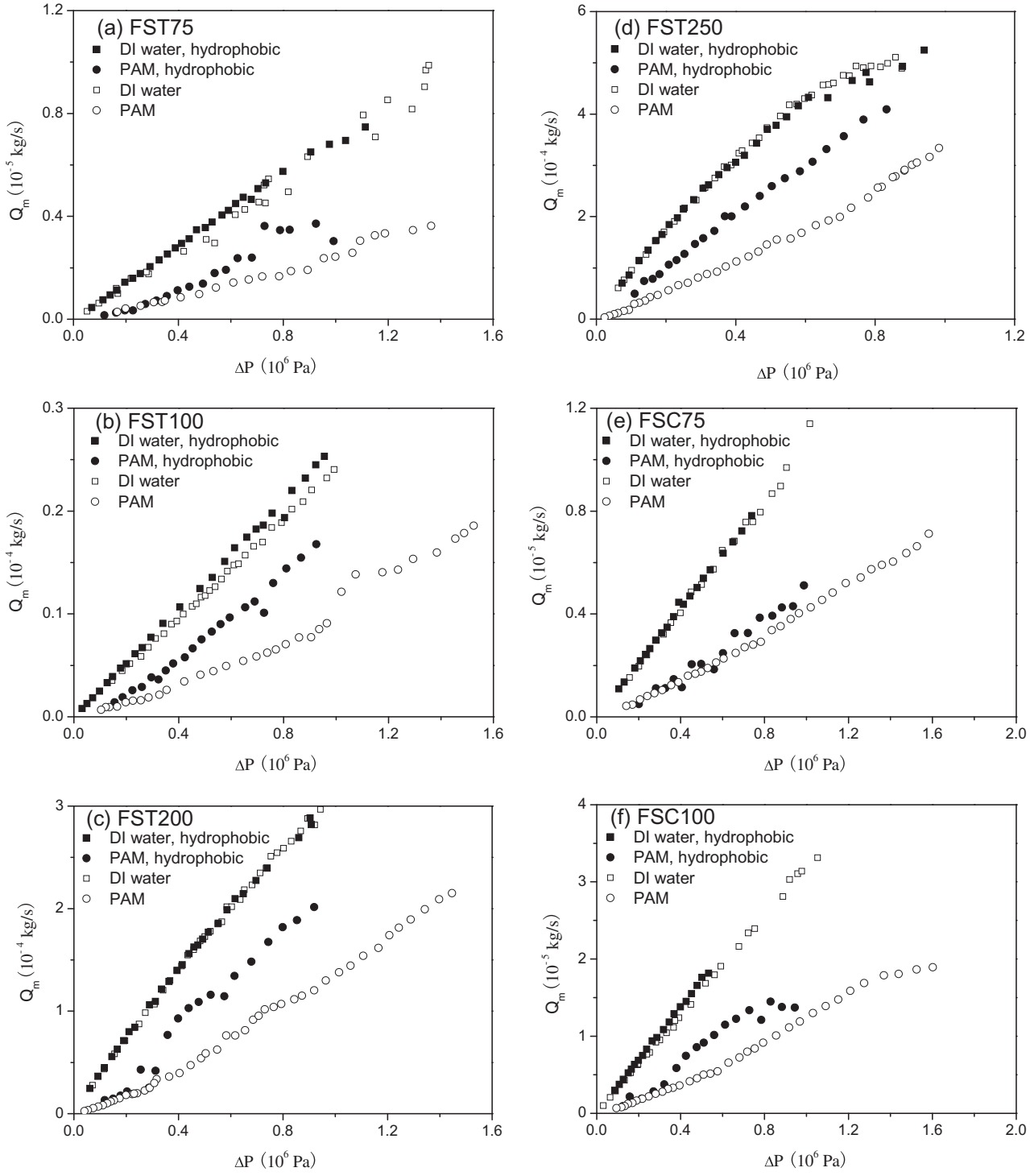


**Fig. 7.** Mass flow rates for the DI water and PAM solution flow in microchannels in hydrophobic condition. The open symbols represent experimental data in untreated microchannels.

for PAM solution increases more evidently in the hydrophobic channels compared to the DI water cases, regardless of the channel type and channel dimension. For DI water, the calculated reduction for the product of Reynolds number and friction factor is up to 10% for FST, 9% for FSC, and 43% for SST, while for the PAM solution flow, the corresponding maximum reduction is 48%, 37%, and 57%, respectively. This result demonstrates that the drag reduction from hydrophobic treatment is more effective for shear thinning non-Newtonian flow. In other words, the shear thinning fluid is more sensitive to the surface wettability compared to the Newtonian fluid. This can be explained as follows. Generally the streamwise velocity profile of shear thinning fluid flow flattens more markedly compared to the typical parabolic distribution of Newtonian flow, in which the near wall streamwise velocity gradient becomes larger for shear thinning fluid. The non-wetting hydrophobic effect can benefit more from this greater near wall velocity gradient since the wall slip velocity is generally proportional to this gradient.

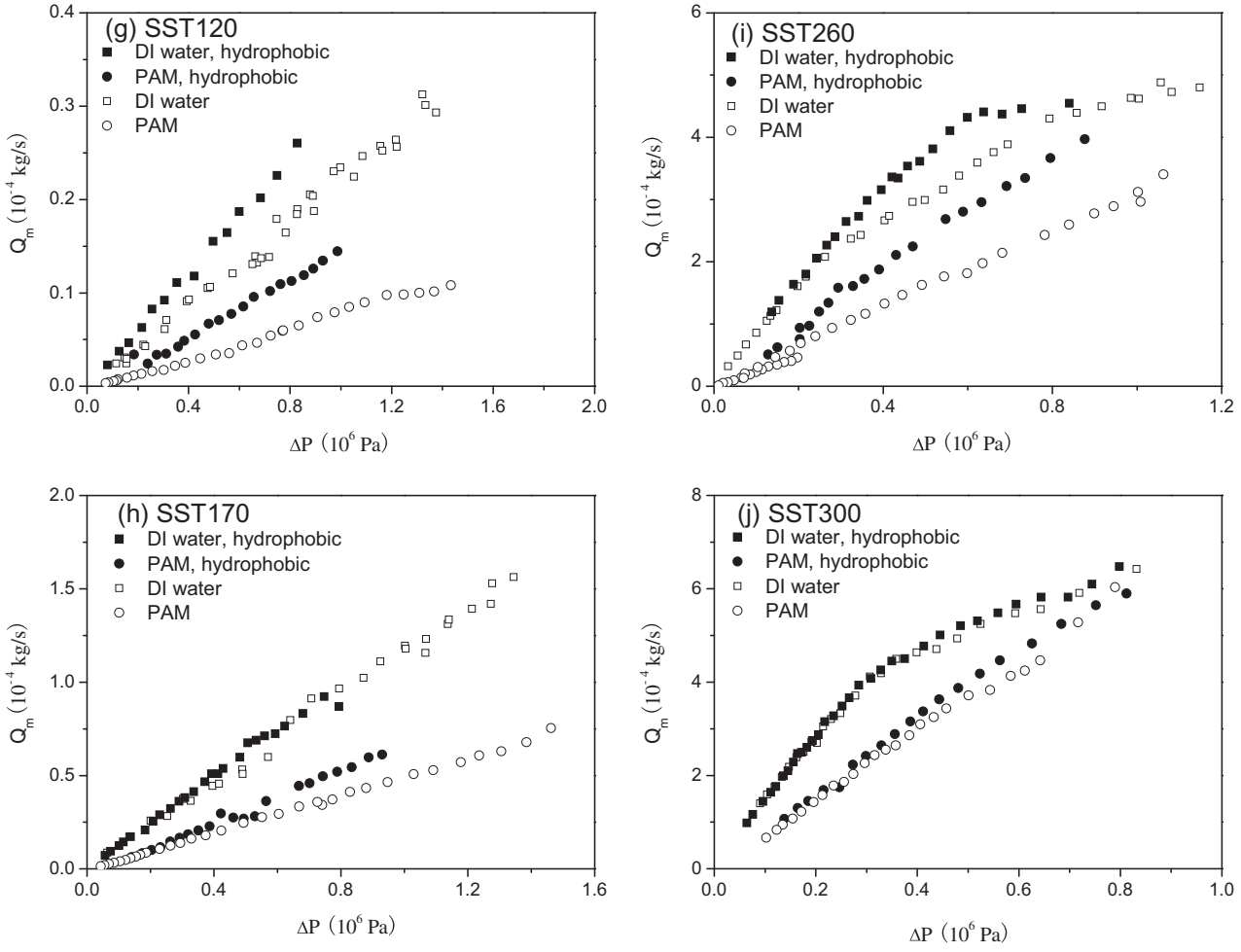


**Fig. 7** (*continued*)

## 4. Conclusions

This article reports experimental results of deionized water flow and shear thinning non-Newtonian fluid flow in both untreated and hydrophobic processed microchannels. The mass flow rates and friction factors for deionized water and PAM solution in fused silica microtubes, fused silica square microchannels, and stainless steel microtubes are presented and discussed. The friction factors and mass flow rates for deionized water flow in smooth fused silica microtubes and fused silica square microchannels are in good agreement with conventional theoretical predictions. The increase of friction factor in rough microchannels is attributed to the relatively higher surface roughness. But the friction factors of shear thinning PAM solution are all larger than conventional theoretical values, which is probably caused by the more evident electroviscous effect on the PAM solution flow in microchannels and by the deviation of the measured rheological data with the conventional rotational rheometer from the real microchannel flow rheological properties. The rheology measurement technique for non-Newtonian fluid microchannel flow faces more challenge.

The hydrophobic processed microchannels are obtained by surface modification processing. The mass flow rates for deionized water and the PAM solution are obtained and compared with the data in untreated microchannels. The results confirm that the hydrophobic microchannel is capable of reducing flow resistance compared with untreated microchannels. For the smaller channel, the drag reduction due to hydrophobic nature is greater. It is also observed that the drag reduction in rough stainless steel microchannels in hydrophobic condition is larger than that for smooth fused silica hydrophobic microchannels. In addition, it is the first time to report that the effect of surface wettability on the shear thinning non-Newtonian fluid flow is more evident than on the Newtonian fluid.

## Acknowledgments

This work was supported by the National Basic Research Program of China (No. 2011CB710702) and by the National Natural Science Foundation of China (No. 51076125). The authors would also like to thank Prof. Rui Zhang in Shanghai Institute of Technology for kind help.

## References

[1] H.A. Stone, A.D. Stroock, A. Ajdari, Engineering flows in small devices, Annu. Rev. Fluid Mech. 36 (2004) 381.
[2] T. Vilkner, D. Janasek, A. Manz, Micro total analysis systems. Recent developments, Anal. Chem. 76 (2004) 3373.
[3] G.M. Whitesides, The origins and the future of microfluidics, Nature 442 (2006) 368.
[4] K. Kang, L.J. Lee, K.W. Koelling, High shear microfluidics and its application in rheological measurement, Exp. Fluids 38 (2005) 222.
[5] N. Srivastava, M.A. Burns, Analysis of non-Newtonian liquids using a microfluidic capillary viscometer, Anal. Chem. 78 (2006) 1690.
[6] X.F. Peng, G.P. Peterson, B.X. Wang, Frictional flow characteristics of water flowing through rectangular microchannels, Exp. Heat Transfer 7 (1994) 249.

[7] G.M. Mala, D.Q. Li, C. Werner, H.J. Jacobasch, Y.B. Nimg, Flow characteristics of water through a microchannel between two parallel plates with electrokinetic effects, Int. J. Heat Fluid Flow 18 (1997) 489.
[8] I. Papautsky, B.K. Gale, S. Mohanty, T.A. Ameel, A.B. Frazier, Effects of rectangular microchannel aspect ratio on laminar friction constant, Proc. Soc. Photo-optical Instrum. Eng. (SPIE) 3877 (1999) 147.
[9] B. Xu, K. Ooti, N. Wong, W.K. Choi, Experimental investigation of flow friction for liquid flow in microchannels, Int. Commun. Heat Mass Transfer 27 (2000) 1165.
[10] W.L. Qu, G.M. Mala, D.Q. Li, Pressure-driven water flows in trapezoidal silicon microchannels, Int. J. Heat Mass Transfer 43 (2000) 353.
[11] G.P. Celata, M. Cumo, M. Guglielmi, G. Zummo, Experimental investigation of hydraulic and single-phase heat transfer in 0.130-mm capillary tube, Microscale Thermophys. Eng. 6 (2002) 85.
[12] D. Brutin, L. Tadrist, Experimental friction factor of a liquid flow in microtubes, Phys. Fluids 15 (2003) 653.
[13] H.Y. Wu, P. Cheng, Friction factors in smooth trapezoidal silicon microchannels with different aspect ratios, Int. J. Heat Mass Transfer 46 (2003) 2519.
[14] J. Judy, D. Maynes, B. Webb, Characterization of frictional pressure drop for liquid flows through microchannels, Int. J. Heat Mass Transfer 45 (2002) 3477.
[15] Z. Li, Y.L. He, G.H. Tang, W.Q. Tao, Experimental and numerical studies of liquid flow and heat transfer in microtubes, Int. J. Heat Mass Transfer 50 (2007) 3447.
[16] G.H. Tang, Z. Li, Y.L. He, C.Y. Zhao, W.Q. Tao, Experimental observations and lattice Boltzmann method study of the electroviscous effect for liquid flow in microchannels, J. Micromech. Microeng. 17 (2007) 539.
[17] A.J. Ghajar, R.P. Rao, W.L. Cook, Experimental investigation of friction factor in the transition region for water flow in minitubes and microtubes, Heat Transfer Eng. 31 (2010) 646.
[18] H.J. Su, H.N. Niu, L.W. Pan, S.D. Wang, A.J. Wang, Y.K. Hu, The characteristics of pressure drop in microchannels, Ind. Eng. Chem. Res. 49 (2010) 3830.
[19] V.M. Aniskin, K.V. Adamenko, A.A. Maslov, Experimental determination of the friction factor coefficient in microchannels, J. Appl. Mech. Tech. Phys. 52 (2011) 18.
[20] P. Wilding, M.A. Shoffner, L.J. Kircka, Manipulation and flow of biological fluids in straight channels micromachined in silicon, Clin. Chem. 40 (1994) 43.
[21] J. Koo, C. Kleinstreuer, Liquid flow in microchannels: experimental observations and computational analyses of microfluidics effects, J. Micromech. Microeng. 13 (2003) 568.
[22] C.H. Choi, K.J.A. Westin, K.S. Breuer, Apparent slip flows in hydrophilic and hydrophobic microchannels, Phys. Fluids 15 (2003) 2897.
[23] J. Ou, B. Perot, J.P. Rothstein, Laminar drag reduction in microchannels using ultrahydrophobic surfaces, Phys. Fluids 16 (2004) 4635.
[24] J. Ou, J.P. Rothstein, Direct velocity measurements of the flow past drag-reducing ultrahydrophobic surfaces, Phys. Fluids 17 (2005) 103606.
[25] B. Woolford, K. Jeffs, D. Maynes, B.W. Webb, Laminar fully developed flow in a microchannel with patterned ultrahydrophobic walls, Proceedings of the ASME Summer Heat Transfer Conference, HT2005-72726, ASME, New York, 2005.
[26] C.H. Choi, U. Ulmanella, J.W. Kim, C.M. Hou, C.J. Kim, Effective slip and friction reduction in nanograted superhydrophobic microchannels, Phys. Fluids 18 (2006) 087105.
[27] D. Maynes, K. Jeffs, B. Woolford, B.W. Webb, Characterization of frictional pressure drop for liquid flows through microchannels, Phys. Fluids 19 (2007) 093603.
[28] D. Byun, J. Kim, H.S. Ko, H.C. Park, Direct measurement of slip flows in superhydrophobic microchannels with transverse grooves, Phys. Fluids 20 (2008) 113601.
[29] B. Woolford, D. Maynes, B.W. Webb, Liquid flow through microchannels with grooved walls under wetting and superhydrophobic conditions, Microfluid. Nanofluid. 7 (2009) 121.
[30] T. Yamada, C. Hong, O.J. Gregory, M. Faghri, Experimental investigations of liquid flow in rib-patterned microchannels with different surface wettability, Microfluid. Nanofluid. 11 (2011) 45.
[31] G.O.F. Parikesit, E.X. Vrouwe, M.T. Blom, J. Westerweel, Biomicrofluidics 4 (2010) 044103.
[32] K. Kozicki, C.H. Chou, C. Tiu, Non-Newtonian flow in ducts of arbitrary cross-sectional shape, Chem. Eng. Sci. 21 (1966) 665.
[33] S.G. Kandlikar, D. Schmitt, A.L. Carrano, J.B. Taylor, Characterization of surface roughness effects on pressure drop in single-phase flow in minichannels, Phys. Fluids 17 (2005) 100606.
[34] A.J. Ghajar, C.C. Tang, W.L. Cook, Experimental investigation of friction factor in the transition region for water flow in minitubes and microtubes, Heat Transfer Eng. 31 (2010) 646.
[35] G.H. Tang, Z. Li, Y.L. He, W.Q. Tao, Experimental study of compressibility, roughness and rarefaction influences on microchannel flow, Int. J. Heat Mass Transfer 50 (2007) 2282.
[36] G.H. Tang, P.X. Ye, W.Q. Tao, Electroviscous effect on non-Newtonian fluid flow in microchannels, J. Non-Newtonian Fluid Mech. 165 (2010) 435.
[37] Q. Li, G.W. He, An atomistic-continuum hybrid simulation of fluid flows over superhydrophobic surfaces, Biomicrofluidics 3 (2009) 022409.
[38] A. Cassie, S. Baxter, Wettability of porous surfaces, Trans. Faraday Soc. 40 (1944) 546.